https://doi.org/10.1007/s41230-019-9083-9

Effect of vibration frequency on primary phase and properties of grey cast iron fabricated by lost foam casting

Bo-tao Xiao[1,2], *Zi-tian Fan[2], Wen-ming Jiang[2], Jun-huai Xiang[1], and Xue-fang Yan[1]

1. Jiangxi Key Laboratory of Surface Engineering, Jiangxi Science and Technology Normal University, Nanchang 330013, China

2. State Key Laboratory of Material Processing and Die & Mould Technology, Huazhong University of Science & Technology, Wuhan 430074, China

Abstract: The properties of gray cast iron (GCI) are affected by density of matrix, size of flake graphite and primary austenite. In this paper, the Y-type specimen of GCI was prepared by lost foam casting (LFC) with and without vibration, and the influence of vibration frequency on the density of matrix, size of primary phase, and properties of the GCI was studied. The results show that the length of the flake graphite and the size of the primary austenite in GCI firstly decrease and then increase with the increase of the vibration frequency. With a vibration frequency of 35 Hz, the length of the flake graphite is the shortest, the primary austenite is the finest and the density of the matrix is the highest. In addition, the tensile strength, elongation and hardness of the GCI firstly increase and then decrease with the increase of the vibration frequency, due to the refinement of the primary phase and the increase of the matrix density. In order to analyze the refinement mechanism of the primary phase of the GCI fabricated by the LFC with vibration, the solidification temperature fields of the GCI fabricated by the LFC with the vibration frequency of 0 and 35 Hz were measured. The results show that the vibration reduces the eutectic point of the GCI and increases the supercooling degree during the eutectic transformation. As a result, the length of the flake graphite and the size of the primary austenite in GCI fabricated by LFC with the vibration frequency of 35 Hz decrease.

Key words: vibration frequency; lost foam casting; grey cast iron; flake graphite; properties

CLC numbers: TG143.2 **Document code:** A **Article ID:** 1672-6421(2020)01-001-07

Lost foam casting (LFC), as a near-net forming method, has been increasingly applied in industry [1-4]. LFC is often used to produce complex cavity structure castings because it has many advantages, such as simple process and low cost. In the process of LFC, the gasification of the foam pattern needs to absorb plenty of heat, which requires a higher pouring temperature of the molten metal than other casting methods [5-6]. At the same time, the dry sand employed in the LFC induces the low cooling rate of the casting. So, coarse microstructure forms due to the higher pouring temperature and lower cooling rate, which therefore deteriorates the properties of the casting. To refine casting microstructure and improve casting properties, many researchers have done a lot of investigations in recent years, and proposed many effective methods for refining grains, such as adding a modifier [7], applying mechanical vibration [8-13], heat treatment [14], and so on. Compared with other methods for refining grains, applying mechanical vibration during the LFC process can refine casting microstructure through a physical method without contamination of the alloy.

Grey cast iron (GCI) has good castability, machinability and wear resistance. It can be used to manufacture complex mechanical parts [15-16], such as cylinders and engine cases by means of LFC. Researchers have carried out some studies on the microstructure refinement of GCI fabricated by LFC [17]. However, reports about GCI fabricated by LFC with vibration are few.

As it is known, the properties of the GCI castings lie on the matrix density, graphite morphology and distribution of the primary phase. In this study, HT100 was selected as the research material. The influences of the vibration frequency on the primary phase and

***Zi-tian Fan**

Male, born in 1962, Professor. Research interests: Precision casting technology of aluminum and magnesium alloys, green casting technology and theory and rapid casting technology.

E-mail: fanzt@hust.edu.cn

Received: 2019-04-28; Accepted: 2019-08-11

properties of the GCI fabricated by the LFC with vibration were investigated.

1 Experimental procedure

The nominal composition of the GCI HT100 is shown in Table 1. Scrap steel, pig iron, ferromanganese, carburant and 75 ferrosilicon was used as raw materials for preparing HT 100 iron liquid. Melting equipment was a one-ton medium-frequency induction furnace. The scrap steel, pig iron and carburant were firstly added into the furnace. When the temperature increased to 1,500 °C, the scrap steel, ferromanganese and ferrosilicon were added into the furnace to adjust the component of the molten metal. Finally, the melt was modified with 75 ferrosilicon and then poured into the sand box. The Y-type specimen of GCI was produced and the thickness of effective portion of the Y-type specimen is 50 mm.

Table 1: Nominal composition of grey cast iron HT100 (wt.%)

C	Si	Mn	S	P	Fe
3.21	2.28	0.63	⩽0.15	<0.30	Bal.

During pouring, the vibration amplitude was kept at 3 mm and the vibration frequencies were 0, 35, 50 and 100 Hz, respectively. The cube specimen for the density measurement was cut using wire cutting and its dimensions were 10.4 mm × 10.4 mm × 10.4 mm. It was then polished to the dimensions of 10 mm × 10 mm × 10 mm using 100, 400 and 800 grit abrasive papers in sequence and the surface was cleaned using ultrasonic cleaning in alcohol. Then the cube mass was measured using a balance, and the density of the GCI was calculated. The average density value was obtained from three specimens for each specified condition. The flake graphite of the GCI before corrosion and the morphology of the primary austenite after corrosion were observed by an optical microscope (OM), and the length of the flake graphite was measured by the optical microscope software system. The etching solution was 4% nitric acid and alcohol solution. The Brinell hardness of the GCI was measured by a HBE-3000A-type Brinell hardness tester with a load of 1,000 kgf and a loading time of 15 s. The average value of the Brinell hardness was taken from three measurements. The mechanical properties of the casting were tested by a SHIMADZU AG-IC universal testing machine. The tensile test was carried out at room temperature at the tensile speed of 1 $mm \cdot min^{-1}$. Then, the fracture morphology was observed by Quanta 200 environmental scanning electron microscopy (ESEM). Finally, the temperature field of the columnar zone during solidification of the GCI fabricated by the LFC with vibration frequency of 0 and 35 Hz was measured by a thermocouple with a diameter of 0.3 mm. The thermocouple wire was welded and embedded into the ceramic tube, and embedded in the foam pattern. The embedded depth of the thermocouple wire was 12.5 mm.

2 Results

2.1 Density of GCI

Figure 1 shows the density of the GCI fabricated by the LFC with different vibration frequencies. It can be seen from Fig. 1, that with the increase of the vibration frequency, the density of the GCI firstly increases and reaches the maximum at the vibration frequency of 35 Hz. Then, the density decreases with the further increasing of the vibration frequency and reaches the minimum at 100 Hz. This value is similar to the GCI fabricated by the LFC without vibration.

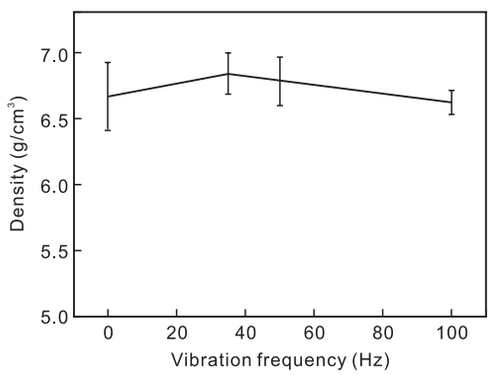

Fig. 1: Density of grey cast iron with different vibration frequencies

2.2 Graphite morphology of GCI

Figure 2 shows the graphite morphology of the GCI fabricated with different vibration frequencies. It can be seen from Fig. 2 and Table 2 that the length of Type A flake graphite in the GCI fabricated by the LFC without vibration is greater than those with vibrations. In addition, some Type C graphites are found in the cast iron fabricated by the LFC without vibration, as shown in Fig. 2(a). As the vibration frequency increases, the length of the flake graphite in the GCI decreases at first and then increases. The length of the flake graphite is the shortest when the vibration frequency is 35 Hz. According to the principles of resonance and vibration solidification, when the vibration frequency applied to the GCI during solidification is close to the natural frequency of the casting system [18], the crystallite breaking is the greatest. Combined with the above analysis, it can be inferred that 35 Hz is close to the low-order natural frequency of the casting system. So, the shortest flake graphite is formed in the GCI fabricated by the LFC with the vibration frequency of 35 Hz.

Table 2: Statistic of Type A graphite length in grey cast iron with different vibration frequencies

Frequency (Hz)	Length of flake graphite (mm)
0	0.36
35	0.19
50	0.27
100	0.33

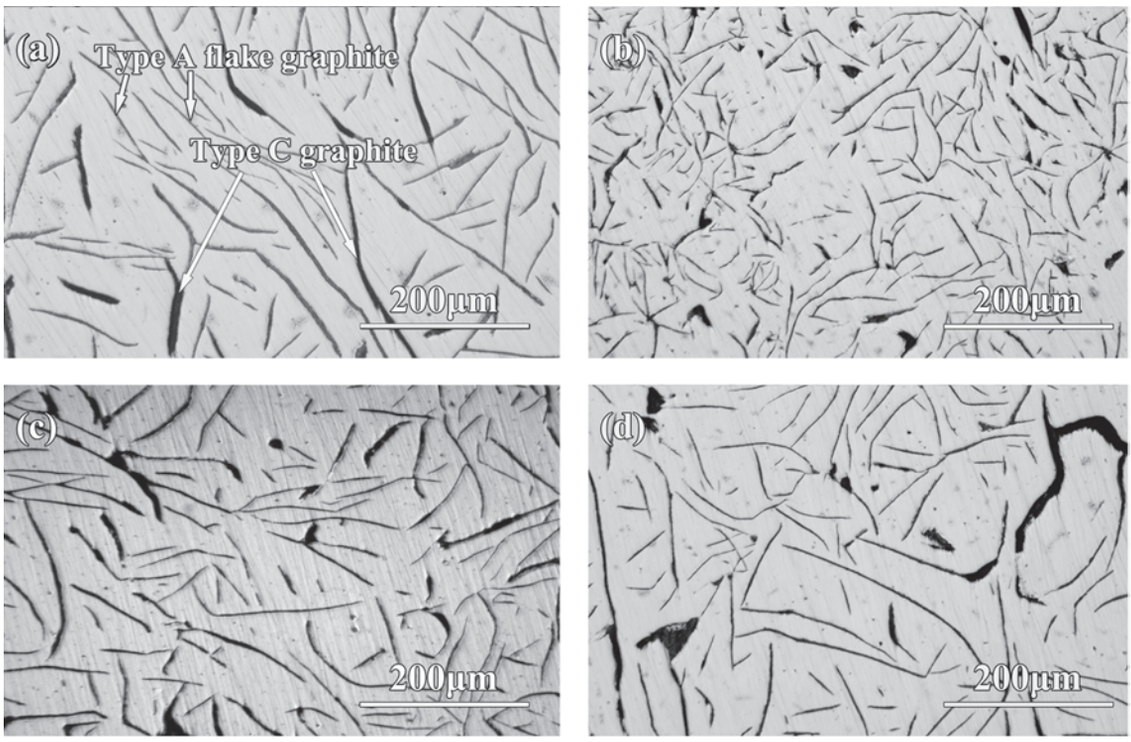

Fig. 2: Graphite morphologies of grey cast iron with different vibration frequencies: (a) 0 Hz; (b) 35 Hz; (c) 50 Hz; (d) 100 Hz

2.3 Primary austenite of GCI

Figure 3 shows the primary austenite morphology of the GCI fabricated with different vibration frequencies. It can be seen from Fig. 3 that the primary austenite dendrite arms are coarser and the secondary dendrite structure is larger in the GCI fabricated without vibration. When the vibration frequency increases to 35 Hz, the size of the primary austenite dendrite decreases, and the primary dendrite and secondary dendrite are finer. When the vibration frequency further increases, the dendrite an the secondary dendrite of the primary austenite become coarser.

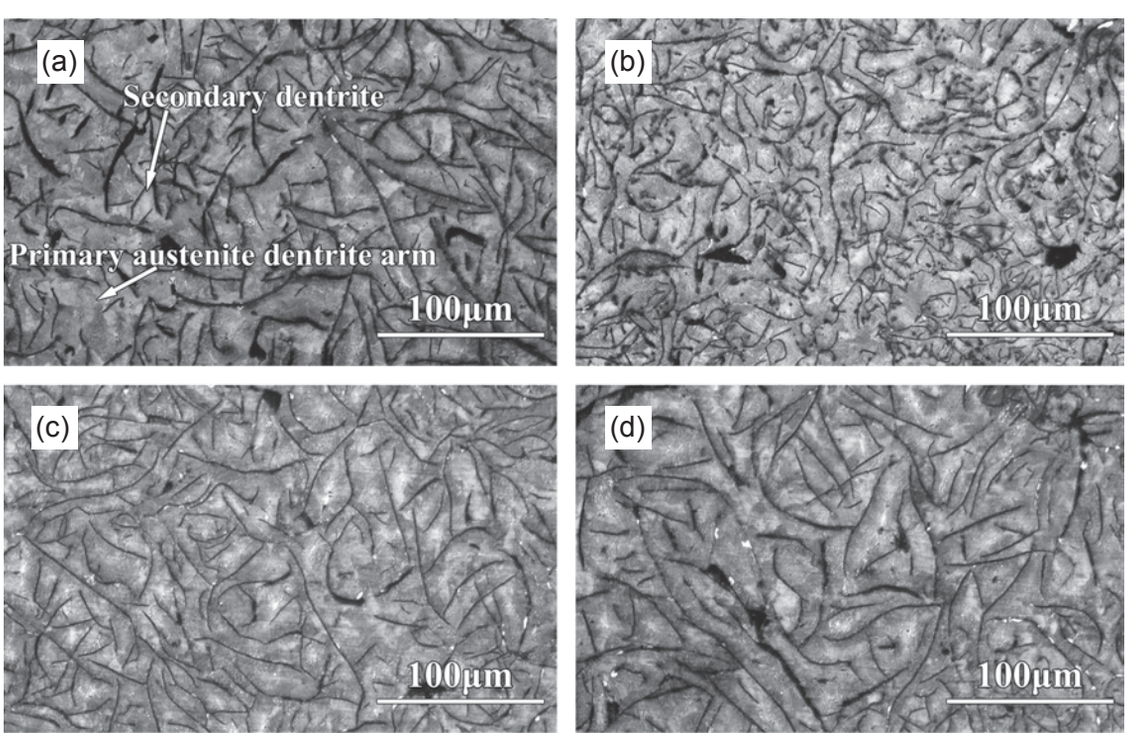

Fig. 3: Primary austenite morphologies of grey cast iron with different vibration frequencies: (a) 0 Hz; (b) 35 Hz; (c) 50 Hz; (d) 100 Hz

2.4 Hardness and tensile properties of GCI

Figure 4 shows the effect of vibration frequency on the hardness of the GCI. It can be seen from Fig. 4 that the Brinell hardness of the GCI increases at first and then decreases with the increase of the vibration frequency, and the Brinell hardness value of the GCI fabricated with the vibration frequency of 35 Hz is the highest. The reason is that the microstructure of the GCI fabricated with the vibration frequency of 35 Hz is the densest compared with that of the GCI fabricated without vibration and with the vibration frequencies of 50 Hz and 100 Hz. The hardness of the GCI fabricated with a vibration frequency of 100 Hz is close to the GCI fabricated without vibration due to their similar densities.

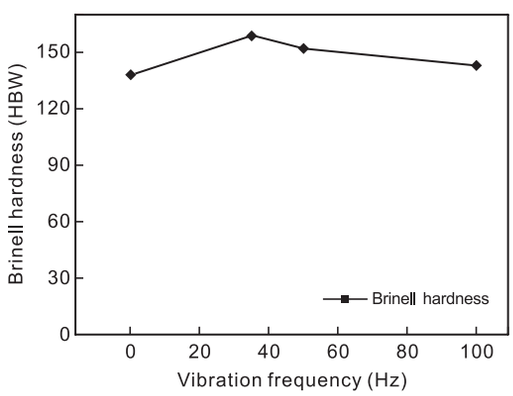

Fig. 4: Brinell hardness of GCI with different frequencies

Figure 5 shows the change of tensile properties of GCI with the vibration frequency. As can be seen from Fig. 5, the tensile strength and elongation of the GCI firstly increase and then decrease with the increase of the vibration frequency. When the vibration frequency is 35 Hz, the tensile strength and elongation of GCI reach the maximum values of 125.99 MPa and 0.89%, and increase 8.6% and 41.27%, respectively, compared to the GCI fabricated without vibration. When the vibration frequency continues to increase to 50 Hz, the tensile strength of the GCI decreases slightly. However, the elongation decreases significantly. Further increase vibration frequency to 100 Hz, and the tensile strength and elongation decrease to 75.76 MPa and 0.43%, respectively, which are lower than for the GCI prepared without vibration.

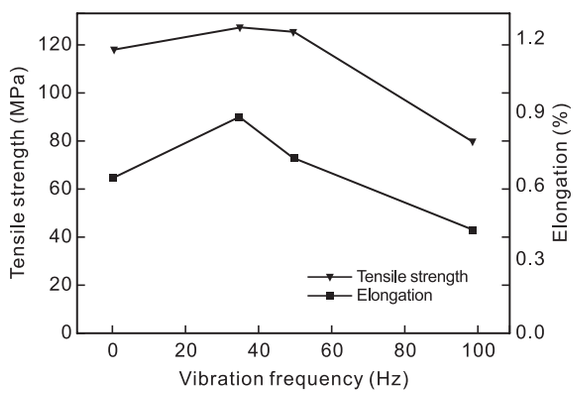

Fig. 5: Properties of GCI with different vibration frequencies

Figure 6 shows the fracture morphology of the GCI fabricated by the LFC with the vibration frequency of 0 and 35 Hz, respectively. As can be seen from Fig. 6, the fracture of the GCI presents the cleavage fracture characteristics of A-type flake graphite and matrix structure, and there are many holes distributed on the fracture surface. He Yi [19] et al. considered that these holes [the circle in Fig. 6(a)] were microporosities formed during the solidification of the GCI, and the fracture of the GCI was attributed to the cleavage of the graphite or the interface separation between graphite and matrix.

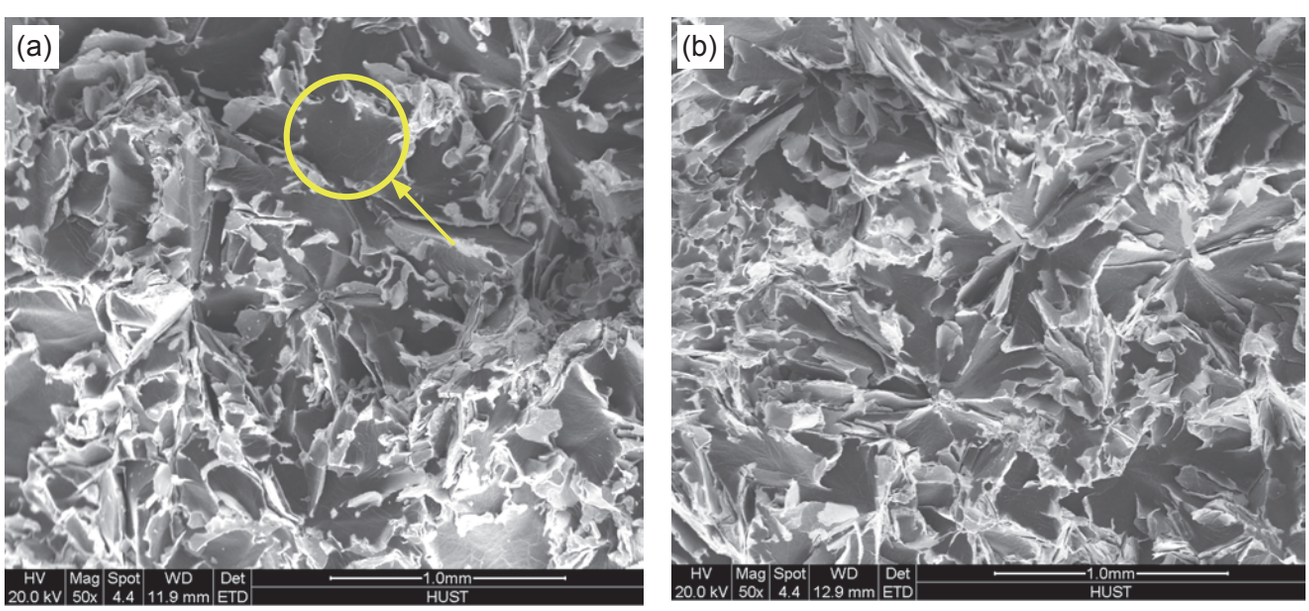

Fig. 6: Fractography of grey cast iron with different vibration frequencies: (a) 0 Hz; (b) 35 Hz

3 Discussions

3.1 Graphite morphology transformation mechanism

According to the carbon equivalent (CE=4.03) of HT100, it belongs to the hypoeutectic alloy. The austenite precipitates first during the solidification process according to the iron-carbon equilibrum diagram. As the temperature decreases to the eutectic point, the eutectic transformation starts, and the eutectic austenite and graphite form. The morphology of the graphite formed in the eutectic reaction depends on the cooling rate of the melt, the supercooling degree of the eutectic transformation, and the nucleation rate of the graphite.

In the LFC process of the GCI, the cooling rate of the melt is fast under the negative pressure, and the primary austenite is formed rapidly. When the temperature of the melt reduces to the eutectic point, the thermal conductivity of the molding sand decreases significantly because the temperature of the dry sand has increased. So, the cooling rate of the molten metal decreases and the supercooling degree during the eutectic transformation decreases, resulting in the formation of the Type A flake graphite.

The composition homogeneity of the GCI is promoted due to the application of the vibration with 35 Hz during the solidification process, which can reduce the concentration gradient of carbon atoms in the melt. Therefore, the driving force of the nucleation and the growth of the graphite are restrained, which result in the shorter and thinner Type A flake graphite.

3.2 Vibration refinement mechanism of primary austenite dendrites

The vibration employed during the solidification of the GCI influences the nucleation and growth of the primary austenite. The vibration induced a cavitation effect in the GCI melt, which caused the formation of a large number of holes. When the hole collapses, the melt around the hole enters the hole and generates a great pressure. This results in the increase of the melting point of the GCI.

In addition, the morphology of the primary austenite is dendrite. The surface curvature difference among the dendrites is great. According to the thermodynamic equation, the change of the equilibrium melting point ΔT_r can be calculated with different curvatures [20],

$$\Delta T_r = \frac{2\sigma T_m V_s K}{\Delta H} \quad (1)$$

where σ is the surface energy of per unit area austenite dendrites, T_m is the melting point of the GCI, V_s is the molar volume of the austenite, K is the surface curvature, ΔH is the melting heat.

It can be seen from Eq. (1) that the change of the equilibrium melting point of the GCI is proportional to the surface curvature of the austenite. The surface curvature of the austenite dendrite is larger at the root and the end of the secondary dendrite arm, while the surface curvature values of other parts change little. Therefore, the change of the melting point is great at the root and the end of the secondary dendrite arm, and the change is small in other positions of the dendrite. The surface curvature of the austenite dendrite is less than 0, and it is known from Eq. (1) that the change of the equilibrium melting point is less than 0. So, the melting point of the austenite dendrite at the root is lower. When the GCI is fabricated by the LFC with vibration, the convection of the molten metal is enhanced. The higher temperature melt flows through the austenite dendrite root, which promotes the remelt of the austenite dendrite, and therefore refines the primary austenite.

The molten metal is a viscous fluid. When the GCI is fabricated by the LFC with vibration, the temperature gradient caused by the convection forms in the molten metal. Meanwhile, the viscous resistance of the metal is altered, and a "viscous shear" is induced in the melt by the vibration. In addition, the influence of the viscous shear is greater between the melt and the solidified austenite dendrites than in GCI fabricated by the LFC without vibration. So the austenite dendrite arm is broken, which results in the increase of the number of the austenite grains in the GCI and the refining of the austenite dendrites.

3.3 Strengthening mechanism of GCI

The main factors affecting GCI properties are the primary phase and density [21]. From the previous analysis, it can be seen that the grains of the primary austenite and dendrites of the GCI fabricated by the LFC without vibration are coarse, and the length and thickness of the Type A flake graphite are larger than those of the samples with vibration. So the properties of the GCI fabricated by the LFC without vibration are poor.

In addition, it can be seen from Fig. 6 that the flower shaped graphite presents on the fracture surface of the GCI. Researchers consider [22] that the stereoscopic morphology of flake graphite is flower-like in the eutectic colony. When the alloy is stretched, the graphite serves as the crack source due to the strength of the graphite being almost zero. With the extension of action time, cracks propagate continuously to the matrix, finally leading to the fracture of the GCI. When the crack spreads in the matrix, the tensile strength of the GCI is increased due to the restraint of the crack by the matrix. However, the tensile strength of the GCI fabricated by the LFC without vibration is low because the Type A flake graphite distributes in the whole matrix of the GCI, and the graphite has a remarkable splitting effect on the matrix.

It can be found that the size of the holes in the GCI fabricated by the LFC without vibration is larger than that with 35 Hz vibration, as shown by the circle in Fig. 6 (a), which leads to the lower density of the GCI. So the GCI fabricated by LFC without vibration has the lower tensile strength compared to the GCI fabricated by LFC with the vibration frequency of 35 Hz. When the vibration frequency is 35 Hz, the microstructure of the GCI is denser than that of the sample without vibration, the type A flake graphite becomes thinner and shorter, and the refining effect of the primary austenite is very obvious. Therefore, the hardness and tensile strength of the GCI are the highest, and the elongation is the highest.

3.4 Thermodynamic of primary austenite dendrites refined by vibration

Figure 7 shows the cooling curve of the columnar crystal area of the GCI fabricated by LFC with the vibration frequencies of 0 and 35 Hz. The definitions of the parameter in the Fig. 7 are shown in reference [23]. It can be seen that the eutectic platform of the GCI with vibration is about 1,110 °C, which is 43 °C lower than the normal eutectic point (1,153 °C), and the eutectic platform of the GCI fabricated by LFC without vibration is about 1,134 °C, which is 19 °C lower than the normal eutectic point (1,153 °C). Comparing the eutectic platform of the GCI obtained by the LFC with and without vibration, it is known that the eutectic platform of the GCI with the vibration frequency of 35 Hz is 24 °C lower than that of the GCI without vibration. Besides, it can be seen from Fig. 7 that the cooling rate of GCI obtained by the LFC with vibration is quicker than that of the GCI obtained by the LFC without vibration, according to the first derivative of the solidification curve. So, the supercooling degree of the GCI obtained by the LFC with vibration is greater.

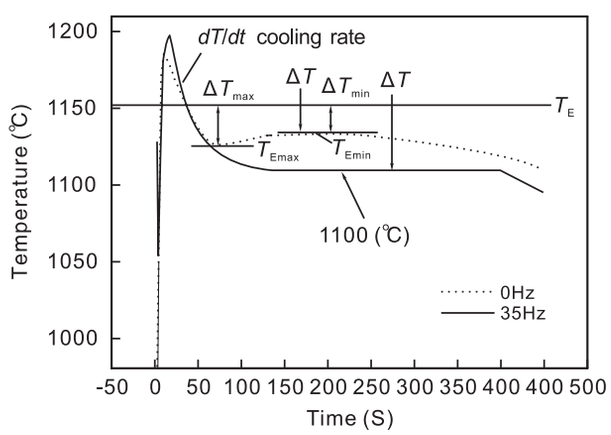

Fig. 7: Cooling curve of columnar zone

According to the critical radius formula for the heterogeneous nucleation of solidification,

$$r^* = \frac{2\sigma_{LC}T_m}{\Delta H_v \Delta T} \quad (2)$$

where, r^* is the critical nucleation radius, σ_{LC} is the surface energy between the liquid phase and the nucleus, T_m is the melting temperature of the metal, ΔH_v is the latent heat of the crystallization per unit volume, and ΔT is the supercooling degree.

It can be known from Eq. (2) that the critical nucleation radius of the grain is inversely proportional to the supercooling degree. The lower the supercooling degree, the larger the critical nucleation radius of the crystal. Therefore, the nucleation of the crystal is restrained. The solidified GCI with the vibration frequency of 35 Hz has a high supercooling degree, and the critical nucleation radius is small, which is beneficial to the nucleation of the primary phase. In addition, the eutectic point of the GCI with the vibration frequency of 35 Hz is low, which reduces the diffusion of atoms in the melt and inhibits the growth of the eutectic austenite and eutectic graphite. Thus, the primary austenite and Type A flake graphite with a smaller size generate. On the contrary, the supercooling degree of the GCI without vibration is lower, which increases the critical nucleation radius of the primary phase and restrains the nucleation of the crystal. Therefore, the amount of the primary phases in the GCI is little. In addition, it can be seen from Fig. 7 that the eutectic point of the GCI fabricated by LFC without vibration is 1,134 °C. So the atomic diffusion speed is increased, and the primary phase generated in the GCI becomes larger than that fabricated by LFC with the vibration frequency of 35 Hz.

4 Conclusions

(1) The density of the grey cast iron (GCI) fabricated by the LFC changes with increasing vibration frequency, and reaches the maximum as the vibration frequency is 35 Hz. With the increase of the vibration frequency, the length of the Type A flake graphite and the size of the primary austenite in the GCI decrease at first and then increase. The length of graphite flake is the shortest and the size of the primary austenite is the smallest for the GCI with a vibration frequency of 35 Hz.

(2) The tensile strength, elongation and hardness of the GCI increase at first and then decrease with the increase of the vibration frequency. When the vibration frequency is 35 Hz, the values of the tensile strength, elongation and hardness of the GCI are the maximum, due to the denser and finer microstructure.

(3) During the LFC process of the GCI, the vibration decreases the eutectic point of the melt and increases the supercooling degree of the solidification, resulting in the grain refinement of the microstructure.

Acknowledgements

This study was financially supported by the National High Technology Research and Development Program of China (No. 2007AA03Z113).

References

[1] Fan Z T, Jiang W M, Liu F C, et al. Status quo and development trend of lost foam casting technology. China Foundry, 2014, 11(4): 296–307.
[2] Fan S, Jiang W M, Li G Y, et al. Fabrication and microstructure evolution of Al/Mg bimetal using a near-net forming process. Materials and Manufacturing Processes, 2017, 32(12): 1391–1397.
[3] KIM Kiyoung, Kyongwhoan LEE. Effect of process parameters on porosity in aluminum lost foam process. Journal of Materials Science & Technology, 2005, 21(5): 681–685.
[4] Jiang W M, Fan Z T. Novel technologies for the lost foam casting process. Frontiers of Mechanical Engineering, 2018, 13(1): 37–47.
[5] Xiao B T, Fan Z T, Jiang W M, et al. Microstructure and mechanical properties of ductile cast iron in lost foam casting with vibration. Journal of Iron and Steel Research International, 2014, 21(11): 1049–1054.

[6] Huang T Y, Huang N Y, Lv Z G. Lost foam casting technology. Beijing: China Machine Press, 2004. (In Chinese)
[7] Zhao Z, Fan Z T, Tang B, et al. Influence of pressure solidification on AZ91D magnesium alloy feeding in lost foam casting process. International Journal of Cast Metals Research, 2011, 24(1): 13–21.
[8] Zhao Z, Fan Z T. Influence of vibration on the heat transfer of lost foam casting filling. Advanced Materials Research, 2011, 418-420: 1618–1621.
[9] Izman S, Shayganpour A, Idris M H. Analysis of the effect of sand size and vibration time on surface roughness in lost foam casting of LM6 alloy by design of experiments. Advanced Materials Research, 2011, 337: 422–425.
[10] Xiao Botao, Fan Zitian, and Liu Xinwang. Grain refinement and hardness of grey cast iron in lost foam casting with mechanical vibration. Metalurgia International, 2013, 18(3): 16–18.
[11] Zhao Z, Fan Z T, Jiang W M, et al. Microstructural evolution of Mg9AlZnY alloy with vibration in lost foam casting during semi-solid isothermal heat treatment. Transactions of Nonferrous Metals Society of China, 2010, 20(3):768–773.
[12] Kisasoz A, Guler K A, Karaaslan A. Influence of orbital shaking on microstructure and mechanical properties of A380 aluminium alloy produced by lost foam casting. Russian Journal of Non-Ferrous Metals, 2017, 58(3): 238–243.
[13] Zou W Q, Zhang Z G, Yang H, et al. Effect of vibration frequency on microstructure and performance of high chromium cast iron prepared by lost foam casting. China Foundry, 2016, 13(4): 248–255.
[14] Jiang W M, Fan Z T, Liu D J. Microstructure, tensile properties and fractography of A356 alloy under as-cast and T6 obtained with expendable pattern shell casting process. Transactions of Nonferrous Metals Society of China, 2012, 22(8): 7–13.
[15] Mirzababaei S, Filip P. Impact of humidity on wear of automotive friction materials. Wear, 2017, 376–377: 717–726.
[16] Xie M G, Zhu C A. Construction and analysis of dynamic solidification curves for non-equilibrium solidification process in lost-foam casting hypoeutectic gray cast iron. China Foundry, 2017, 14(3): 176–183.
[17] Hu Z J, Cheng H F, Xie M G, et al. Influence of inoculation method on microstructure and performance of gray iron produced via lost foam casting. Foundry Technology, 2011, 32(1): 15–19. (In Chinese)
[18] Dong X W, Hu Z J, Zhan J H, et al. Effect of exciting frequency on the residual stress of the vibrating solidification casting. Foundry, 2000, 49(11): 816–818. (In Chinese)
[19] He Y, Shen B L, Li L, et al. An investigation on fracture morphology differences between gray irons with A-Type and D-Type graphite. Modern Cast Iron, 2009, 2: 85–88. (In Chinese)
[20] Song L B. Effect of mechanical vibration on microstructure and properties of AZ91D magnesium alloy. Taiyuan University of Science & Technology, 2011. (In Chinese)
[21] Sun S C, Fu M X, Zhou B Y, et al. Primary austenite and graphite microstructure in gray cast iron. Journal of Jiangsu Institute of Technology, 1991, 1: 121–122. (In Chinese)
[22] He R T, Long R, Gu J L, et al. The morphology characteristics on fracture surface and behavior in fracture process of flake graphite. Journal of Luoyang Institute of Technology, 1987, 2: 11–19. (In Chinese)
[23] Stefanescu D M. Thermal analysis- theory and applications in metalcasting. International Journal of Metalcasting, 2015, 9(1): 7–22.